JCI The Journal of Clinical Investigation

Mesodermal *Pten* inactivation leads to alveolar capillary dysplasia-like phenotype

Caterina Tiozzo, … , Saverio Bellusci, Parviz Minoo

J Clin Invest. 2012;122(11):3862-3872. https://doi.org/10.1172/JCI61334.

Research Article **Pulmonology**

Alveolar capillary dysplasia (ACD) is a congenital, lethal disorder of the pulmonary vasculature. Phosphatase and tensin homologue deleted from chromosome 10 (*Pten*) encodes a lipid phosphatase controlling key cellular functions, including stem/progenitor cell proliferation and differentiation; however, the role of PTEN in mesodermal lung cell lineage formation remains unexamined. To determine the role of mesodermal PTEN in the ontogeny of various mesenchymal cell lineages during lung development, we specifically deleted *Pten* in early embryonic lung mesenchyme in mice. Pups lacking*Pten* died at birth, with evidence of failure in blood oxygenation. Analysis at the cellular level showed defects in angioblast differentiation to endothelial cells and an accompanying accumulation of the angioblast cell population that was associated with disorganized capillary beds. We also found decreased expression of Forkhead box protein F1 (*Foxf1*), a gene associated with the ACD human phenotype. Analysis of human samples for ACD revealed a significant decrease in PTEN and increased activated protein kinase B (AKT). These studies demonstrate that mesodermal PTEN has a key role in controlling the amplification of angioblasts as well as their differentiation into endothelial cells, thereby directing the establishment of a functional gas exchange interface. Additionally, these mice could serve as a murine model of ACD.

Mesodermal *Pten* inactivation leads to alveolar capillary dysplasia-like phenotype

Caterina Tiozzo,[1,2] Gianni Carraro,[2,3] Denise Al Alam,[2] Sheryl Baptista,[2] Soula Danopoulos,[2] Aimin Li,[1] Maria Lavarreda-Pearce,[2] Changgong Li,[1] Stijn De Langhe,[4] Belinda Chan,[1] Zea Borok,[5] Saverio Bellusci,[2,3] and Parviz Minoo[1]

[1]Department of Pediatrics, Division of Newborn Medicine, University of Southern California, Children's Hospital, Los Angeles, California, USA. [2]Developmental Biology Program, Saban Research Institute of Children's Hospital Los Angeles, Los Angeles, California, USA. [3]University of Giessen Lung Center, Excellence Cluster in Cardio-Pulmonary Systems, Member of the German Lung Center, Department of Internal Medicine II, Giessen, Germany. [4]Department of Pediatrics, Division of Cell Biology, National Jewish Health, Denver, Colorado, USA. [5]Will Rogers Institute Pulmonary Research Center, Division of Pulmonary Critical Care Medicine, Department of Medicine, University of Southern California, Los Angeles, California, USA.

Alveolar capillary dysplasia (ACD) is a congenital, lethal disorder of the pulmonary vasculature. Phosphatase and tensin homologue deleted from chromosome 10 (*Pten*) encodes a lipid phosphatase controlling key cellular functions, including stem/progenitor cell proliferation and differentiation; however, the role of PTEN in mesodermal lung cell lineage formation remains unexamined. To determine the role of mesodermal PTEN in the ontogeny of various mesenchymal cell lineages during lung development, we specifically deleted *Pten* in early embryonic lung mesenchyme in mice. Pups lacking *Pten* died at birth, with evidence of failure in blood oxygenation. Analysis at the cellular level showed defects in angioblast differentiation to endothelial cells and an accompanying accumulation of the angioblast cell population that was associated with disorganized capillary beds. We also found decreased expression of Forkhead box protein F1 (*Foxf1*), a gene associated with the ACD human phenotype. Analysis of human samples for ACD revealed a significant decrease in PTEN and increased activated protein kinase B (AKT). These studies demonstrate that mesodermal PTEN has a key role in controlling the amplification of angioblasts as well as their differentiation into endothelial cells, thereby directing the establishment of a functional gas exchange interface. Additionally, these mice could serve as a murine model of ACD.

Introduction

Understanding of the molecular mechanisms regulating formation of the pulmonary vascular system has advanced in recent years (1–4). However, the complex regulatory network that controls lung vasculogenesis and involvement of mesenchymal progenitors in pulmonary vascular diseases remains unclear. Developmental abnormalities of the pulmonary circulation contribute to significant neonatal morbidity due to disorders such as alveolar capillary dysplasia (ACD) and bronchopulmonary dysplasia (BPD) (5). Congenital ACD is a disorder of pulmonary vascular development seen in neonates, with irreversible persistent pulmonary hypertension and 100% mortality (6). The initial presentation is identical to that of severe idiopathic pulmonary hypertension of the newborn. However, infants with ACD do not respond or respond only transiently to therapies that are usually effective in reversing this condition. Infants with ACD do not improve despite maximal support in the intensive care nursery, including mechanical ventilation, nitric oxide, and extracorporeal membrane oxygenation (ECMO). ACD is also associated with BPD, a chronic lung disease that affects almost 10,000 babies every year in the United States. To date, the underlying etiological factors of these diseases are unknown, and therefore there are no available diagnostic tests and therapeutic options. For these reasons, a better understanding of this process is necessary and mandatory in order to establish urgently needed clinical treatment remedies.

Phosphatase and tensin homologue deleted from chromosome 10 (PTEN) is an important modulator of cell-fate determination and governs normal vascular development. PTEN is a lipid phosphatase involved in the PI3K pathway and is therefore connected with growth factor signaling pathways (7). By controlling the amount of phosphatidylinositol-3,4,5-triphosphate (PIP3), PTEN is involved in several cellular functions, such as cell migration, organ size control, proliferation, and apoptosis (8).

In previous studies, we have shown that absence of *Pten* in the lung epithelium leads to an increase of epithelial progenitor cells and possibly increased susceptibility to lung cancer, but also to protection against lung injury (9). Hamada et al. (10) reported that mice with an endothelial cell–specific mutation of *Pten* displayed embryonic lethality due to bleeding and cardiac failure caused by impaired recruitment of pericytes and VSMCs to blood vessels. In addition, Deleris et al. (11) showed that PTEN is also expressed and active in VSMCs controlling the level of PIP3 and therefore potentially controlling VSMC proliferation. To date, the role of *Pten* in the lung mesenchyme has remained elusive.

In this study, we examined the consequences of mesenchymal-specific deletion of *Pten* in the embryonic lung using a *Dermo1-Cre* mouse line that drives Cre expression in the lung mesenchyme as early as E11.5 (2, 12). We observed that the $Pten^{fl/fl;Dermo\text{-}Cre}$ animals died at birth for lack of blood oxygenation. We show that mesodermal PTEN plays a key role in controlling the amplification of angioblasts as well as their differentiation into endothelial cells, thereby allowing the establishment of a functional gas exchange interface. The $Pten^{fl/fl;Dermo\text{-}Cre}$ mice generated in the current study represent a potential murine model of ACD.

Authorship note: Parviz Minoo and Saverio Bellusci contributed equally to this work.

Conflict of interest: The authors have declared that no conflict of interest exists.

Citation for this article: *J Clin Invest.* 2012;122(11):3862–3872. doi:10.1172/JCI61334.

Table 1
Pten$^{fl/fl;Dermo1\text{-}Cre}$ mice suffer embryonic lethality

	Total embryos	*Pten*$^{fl/fl;Dermo1\text{-}Cre}$
E12.5	65	19 (29%)
E.15.5	63	16 (25%)
E18.5	311	67 (21%)
P21	121	0 (0%)

Pten$^{fl/fl;Dermo\text{-}Cre}$ mice display embryonic and neonatal mortality. Genotyping of *Pten*$^{fl/fl;Dermo\text{-}Cre}$ mice at different gestational ages. At E12.5 and E15.5, the mutants accounted for, respectively, 29% (19 out of 65) and 25% (16 out of 63) of the total embryos, while at E18.5, their number was 21% (67 out of 311), indicating embryonic lethality between E15.5 and E18.5. At P21, no mutant mice were detected (total 121). *Pten*$^{fl/fl;Dermo\text{-}Cre}$ mice came from female *Pten*$^{fl/fl}$ and male *Pten*$^{fl/+;Dermo\text{-}Cre}$ breeding.

Results

Mesodermal-specific inactivation of Pten causes embryonic and immediate postnatal lethality. We used *Dermo1-Cre* to inactivate *Pten* via deletion of exon 5. The expression pattern and efficiency of *Dermo1-Cre* in the lung were examined by crossing *Dermo1-Cre* mice with *ROSA26R-LacZ* reporter mice (Supplemental Figure 1G; supplemental material available online with this article; doi:10.1172/JCI61334DS1). As reported (1), LacZ activity was widespread throughout the pulmonary mesenchyme, but did not include the endothelial cells in the lung vasculature (Supplemental Figure 1G).

To accomplish mesodermal inactivation of *Pten* in the lung, heterozygous *Pten*$^{fll/+;Dermo\text{-}Cre}$ males were crossed with *Pten*$^{fl/fl}$ females. The offspring (n = 121) were genotyped using PCR analysis of tail DNA at 3 weeks of age. No *Pten*$^{fl/fl;Dermo\text{-}Cre}$ (i.e., homozygous deletion) offspring were detected. We therefore determined the percentile of homozygous mutants and WT embryos at different gestational ages (Table 1). At E12.5 and E15.5, the mutants accounted for 29% (19 out of 65) and 25% (16 out of 63), respectively, of the total number of embryos, while at E18.5, their number was reduced to 21% (67 out of 311), indicating embryonic lethality between E15.5 and E18.5. During embryonic stages, the mutants showed a wide range of phenotype, from a lack of vascularization in entire embryos at E15.5 (Supplemental Figure 2, A and B; 7 out of 16 mutant embryos: 44%) to a hemorrhagic phenotype at E18.5 (Supplemental Figure 2, C and D; 10 out of 67 mutant embryos: 15%). All other mutant embryos with less severe phenotype died within 2 to 3 hours postnatally, displaying cyanosis, chest retractions, and dyspnea (Supplemental Figure 2E). Measurements of blood oxygenation (Figure 1I) showed statistically significant differences between *Pten*$^{fl/fl}$ (controls) and *Pten*$^{fl/fl;Dermo\text{-}Cre}$ newborns (97% ± 3.7% vs. 73% ± 8.2%, P < 0.01). A careful study of the embryos at E15.5 showed lack of vascularization in other organs, such as limbs and liver (Supplemental Figure 3, A–J).

To validate *Pten* inactivation in the pulmonary mesoderm, we compared expression patterns and levels of PTEN and phosphorylated protein kinase B (p-AKT) in mutant versus WT lungs by immunohistochemistry (IHC) in E18.5 embryos (Supplemental Figure 1, A–D). When compared with controls, mutant lungs showed an overall decreased PTEN (Supplemental Figure 1, compare B and A). However, recombination was not complete, as some mesodermal-derived cells remained PTEN positive, displaying nuclear immunoreactivity (Supplemental Figure 1B). Consistent with the specificity previously documented for *Dermo1-Cre* activity, epithelial PTEN immunoreactivity was unperturbed (Supplemental Figure 1B). Using E18.5 lung RNA, quantitative RT-PCR (qRT-PCR) was performed to confirm interruption of *Pten* gene expression (Supplemental Figure 1E). In *Pten*$^{fl/fl;Dermo\text{-}Cre}$ lungs, *Pten* mRNA was decreased (0.58% ± 0.07%, P < 0.01) compared with *Pten*$^{fl/fl}$ controls (n = 4 per group). Finally, Western blot analysis (Supplemental Figure 1F) showed that PTEN was reduced in the mutant lungs compared with controls (0.14 ± 0.01 vs. 0.51 ± 0.09, n = 4 per group, P < 0.05).

PTEN is a lipid phosphatase that regulates PIP3 levels, thus negatively modulating the PI3K/AKT pathway. IHC revealed an increase of p-AKT in mutant lungs compared with controls (Supplemental Figure 1, D vs. C), further confirming deregulation of the PI3K pathway. Western blot analysis of E18.5 whole-lung extracts (n = 4 for each group) confirmed increased p-AKT in mutant versus control lungs (0.03 ± 0.004 vs. 0.012 ± 0.00053 P < 0.05; Supplemental Figure 1F).

To determine the potential structural causes underlying reduced blood oxygenation in the mutant newborns, histology of E18.5 lungs using H&E staining was examined (Figure 1, A–D). While no branching or other significant gross structural abnormalities were observed (Figure 1, B and D vs. A and C), closer examination of mutant lungs (Figure 1D) revealed a hypercellular mesenchymal compartment compared with the controls (Figure 1C). This observation was confirmed by detection of mesenchymal-specific increased cell proliferation, as documented by E-cadherin (E-CAD)/PH3 immunofluorescence (Figure 1, E and F). Due to increased mesodermal cells, the total number of E-CAD–negative cells was higher in mutant lungs compared with controls (Figure 1G, 363.5 ± 20.7 vs. 223.1 ± 10.2, P < 0.01). The number of E-CAD–negative/PH3-positive cells was nearly 6-fold higher in mutant versus control lungs (17.8% ± 1.1% versus 3.15% ± 0.8% respectively n = 3, P < 0.01) (Figure 1H).

Mesodermal Pten deficiency affects vasculogenesis. Differentiated endothelial cells, identified by PECAM, are derived from mesodermally derived progenitor cells, which express *Flk1* (*Vegfr2*). These progenitors can be identified in embryonic lungs starting as early as E10.5 (13). Their formation is tightly associated with mesenchymal and epithelial development during branching morphogenesis (1). As defective pulmonary vascular formation can cause hypoxemia, we examined PECAM in E15.5 lungs by IHC (Figure 2, A and B). In *Pten*$^{fl/fl;Dermo\text{-}Cre}$ lungs, there was significant reduction in distal capillary network density compared with *Pten*$^{fl/fl}$ controls, the latter exhibiting normal dense capillary plexus adjacent to the developing airway epithelium. In E18.5 control lungs (Figure 2C), red blood cell–containing capillaries were found in close spatial proximity to the alveolar-air interface. This coupling is critical for normal gas exchange. In contrast, the capillary network in *Pten*$^{fl/fl;Dermo\text{-}Cre}$ lungs was distinctly abnormal, with clear uncoupled capillary/airway network, rendering pulmonary units incapable of efficient gas exchange (Figure 2D). Statistical analysis of the distance between the capillaries and the lumen of airways showed significant increase in the mutant versus control lungs (Figure 2E, 3.3 μm ± 0.3 μm vs. 0.9 μm ± 0.1 μm, P < 0.01). More detailed study of the lung ultrastructure showed mutant alveolar spaces were frequently lined by cuboidal cells with "immature" lamellar bodies, while the type 2 cells in control lungs contained surfactant. To better understand the mechanism underlying this phenotype, we assessed the levels of *Vegfa*, *Flt1* (*Vegfr1*), and *Flk1* (*Vegfr2*) at E18.5 by qRT-PCR. *Vegfa*

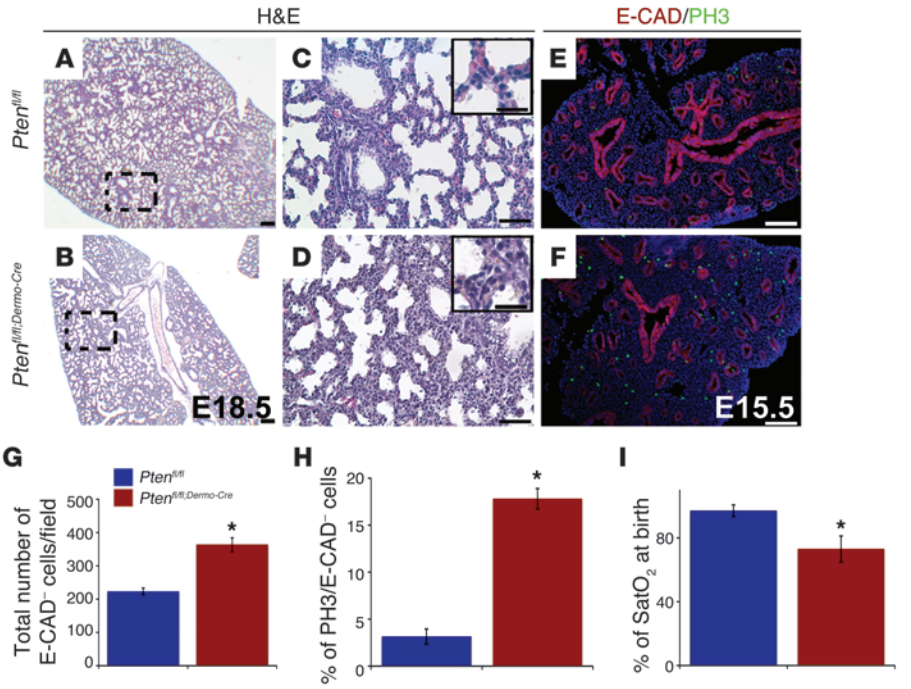

Figure 1

Absence of *Pten* in the mesenchyme does not affect lung morphogenesis, but leads to increased mesenchymal cell proliferation. (**A**–**D**) Histological analysis of E18.5 lungs. $Pten^{fl/fl}$ and $Pten^{fl/fl;Dermo\text{-}Cre}$ lungs were H&E stained. Representative WT and KO sections are shown. No macroscopic differences were detected between the WT and mutant embryos except for increased cell density (**D** versus **C**). Scale bars: 100 μm (**A** and **B**); 50 μm (lower magnification), 20 μm (higher magnification) (**C** and **D**). (**E** and **F**) Increased cell proliferation in *Pten* conditional KO (cKO) mice compared with controls. IF for E-CAD and PH3, showing increased proliferation in $Pten^{fl/fl;Dermo\text{-}Cre}$ mesenchyme (**F**) compared with $Pten^{fl/fl}$ (**E**). Scale bars: 50 μm. (**G**) Total number of E-CAD–negative cells was counted. Data are expressed as mean total lung cells ± SEM for 3 mice/group. $^*P < 0.01$, Student's *t* test. (**H**) Increased proliferation (PH3-positive cells) of total cell numbers in the E-CAD–negative population of the cKO mice. Data expressed as percentage of PH3-positive cells and E-CAD–negative over the total E-CAD–negative cells in 3 mice/group. (**I**) Statistical analysis of the $SatO_2$ in control and mutant mice at birth, confirming hypoxia in mutants immediately after birth.

was reduced in mutant lungs compared with controls (Figure 3A, 0.39 ± 0.03 vs. 1, $P < 0.01$) as was *Flt1* (Figure 3A, 0.73 ± 0.08 vs. 1, $P < 0.05$). There was also a quantifiable increase in *Flk1* mRNA in $Pten^{fl/fl;Dermo\text{-}Cre}$ lungs (Figure 3A, 11.61 ± 2.6 vs. 1, $P < 0.05$). Furthermore, *Pecam* mRNA was decreased in the mutant lungs versus controls (Figure 3A, 0.47 ± 0.1 vs. 1, $P < 0.01$), supporting the IHC data shown in Figure 2, A and B.

Finally, qRT-PCR for *Vegfa,* using mRNA from E15.5 and E18.5 isolated fibroblasts, revealed no statistically significant difference between control and mutant cells (Figure 3F, E15.5: 1.067 ± 0.5 vs. 1, $P > 0.05$; E18.5: 1.16 ± 0.6 vs. 1, $P > 0.05$). Thus, as the mesenchyme does not appear to be involved, the data suggest the epithelium as the compartment in which the decrease in *Vegfa* occurs. This conclusion was validated via immunofluorescent (IF) for VEGFA plus E-CAD, which showed markedly decreased VEGFA in E-CAD–positive cells in the mutant lungs (compare Figure 3, H and G).

One possibility for the changes in *Flk1* and *Flt1* levels is that mesodermal-specific *Pten* inactivation affects endothelial cell differentiation even though *Dermo1-Cre* as shown in this and other reports is not active in this cell lineage (1, 2). Therefore, we examined the differentiation of endothelial cells by generating triple-transgenic mice consisting of the $Pten^{fl/fl;Dermo\text{-}Cre}$ embryos in a $Flk1^{LacZ}$ reporter background (14). In these mice, *LacZ* is under the control of the endogenous *Flk1* promoter. *Flk1* is an early marker of angioblasts, and its expression is maintained in mature endothelial cells together with *Flt1* (14). Significant increase in *Flk1*-driven LacZ activity was found throughout the entire mutant lungs compared with controls (Figure 3, C vs. B). Ablation of mesodermal *Pten* therefore does not interfere with specification and amplification of angioblasts. However, analysis of PECAM, a marker for mature endothelial cells in $Pten^{fl/fl;Dermo\text{-}Cre}$ lungs, revealed impaired differentiation of angioblasts into mature endothelial cells and blood vessels when compared with controls. We therefore analyzed sections from E18.5 $Pten^{fl/fl;Dermo\text{-}Cre};Flk1^{LacZ}$ and $Pten^{fl/fl};Flk1^{LacZ}$ lungs and examined them for PECAM. The mutant lungs showed increased FLK1-positive/PECAM-negative cells (Figure 3, E vs. D), confirming the conclusion that angioblasts are indeed increased in the mutant lungs. Finally, we examined the tridimensional structure of lung vasculature by injecting FITC leptin in the left ventricle of mutant and control hearts, observing again a significant defect in vasculogenesis in mutant versus controls (Supplemental Video 1). In sum, the results strongly support the conclusion that lack of PTEN in the mesodermal lineages inhibits differentiation of angioblasts into mature endothelial cells.

Dermo1-Cre–mediated Pten inactivation affects ontogeny of mesodermal cell lineages. To determine the impact of mesodermal *Pten* inactivation on the emergence and differentiation of lung mesenchymal cell lineages, expression of a number of cell markers was examined by IHC and qRT-PCR. Immunofluorescence showed decreased α-SMA, a smooth muscle differentiation marker in E18.5 mutant lungs (Figure 4, B versus A). Adipose differentiation-related protein (ADRP), a lipid droplet–associated protein expressed early during adipose differentiation and a marker of lipofibroblasts in the lung, was decreased in $Pten^{fl/fl;Dermo\text{-}Cre}$ lungs compared with $Pten^{fl/fl}$ (Figure 4, D vs. C). Finally, in E18.5 lungs, the capillary network was misaligned with corresponding respiratory airways (i.e., airway/capillary uncoupling or dysplasia) in the mutants, as shown by IHC for PECAM (Figure 4, F vs. E). Interestingly, double IHC for PDGFrα (marker for fibroblasts) and E-CAD (marker for epithelial cells) and Sirius red staining for collagen, a product of fibroblasts, showed increased PDGFrα-positive/E-CAD–negative cells (Figure 4, H vs. G, statistical analysis: Figure 4L, 2% ± 0.2% vs. 11% ± 0.02%, $P < 0.01$). Collagen deposition was also increased in the $Pten^{fl/fl;Dermo\text{-}Cre}$ lungs compared with controls (Figure 4, J vs. I). These IHC results were validated by qRT-PCR for the different cell lineage markers, which showed a trend toward reduced expression

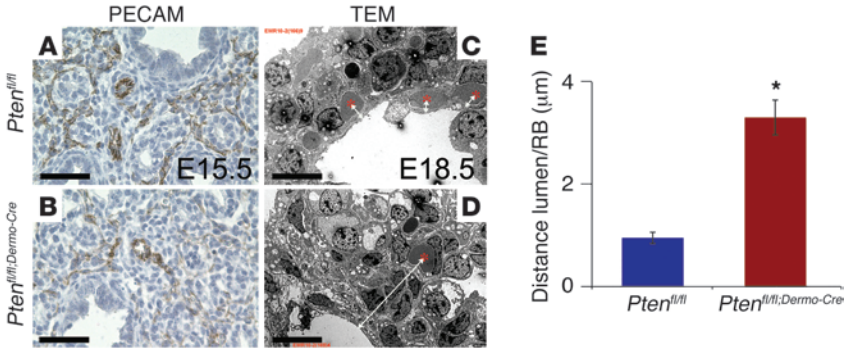

Figure 2
Abnormal airway capillary coupling. (**A** and **B**) IHC for PECAM, an endothelial marker, showing defect in capillary formation at E15.5. (**C** and **D**) Transmission electron microscopy confirmed increased distance (white arrows) between capillaries (red asterisks: blood cells) and alveoli in mutant lungs. (**E**) The airway-capillary distance was significantly thicker in mutant lungs (*$P < 0.01$, $n = 3$). Scale bars: 50 μm (**A** and **B**); 5 μm (**C** and **D**).

of α-*Sma* (Figure 4K, 0.52 ± 0.3 vs. 1, $P > 0.05$) and *Adrp* (Figure 4K, 0.03 ± 0.00001 vs. 1, $P < 0.01$) in primary cultures of E18.5 mutant fibroblasts compared with controls. *Pecam* was also reduced in the mutant versus control lungs (Figure 4K, 0.47 ± 0.1 vs. 1, $P < 0.01$). Collagen 1 by Sircol assay was increased in the mutant lungs versus controls (Figure 4M, 83.13 μg/ml ± 7.2 vs. 39.23 μg/ml ± 6.3, $P < 0.01$).

Using flow cytometry to confirm these observations, we gated the mesenchymal progenitor cells by Hoechst staining in E17.5 mutant and control lungs ($n = 14$ for each). In the embryonic lung, 2 subtypes of side populations are thought to exist (15). One is identified as $CD45^-CD31^+$E-SP cells, believed to differentiate into endothelial cells. The other is identified by markers $CD45^-CD31^-$E-SP, with a gene profile consistent with a smooth muscle precursor (15). At E17.5, we observed more than a 5-fold increase in the number of $CD45^-CD31^+$E-SP and $CD45^-CD31^-$E-SP cell populations in $Pten^{fl/fl;Dermo\text{-}Cre}$ lungs versus controls (respectively 1.1% versus 0.2% and 2.9% versus 0.5%) (Figure 4N). Therefore, mesenchymal PTEN controls the size of the 2 putative lung mesenchymal progenitor cell populations.

Early mesodermal Pten inactivation leads to increased FGF10 signaling. AKT-mediated phosphorylation of β-catenin (β-CAT) on Ser552 drives nuclear localization of β-CAT and activation of WNT target genes. To determine whether mesodermal *Pten* inactivation increases phosphorylation of β-CAT on Ser552 in the mesenchyme, we performed IHC for E-CAD and $\beta\text{-CAT}^{Ser552}$ (Figure 5, G and H), the form of β-CAT specifically phosphorylated by the PTEN/AKT pathway (16). We found significantly increased E-CAD–negative/ $\beta\text{-CAT}^{Ser552}$–positive cells in mutant lungs compared with controls (Figure 5J, 1.3% ± 0.1 vs. 0.3% ± 0.1, $P < 0.01$). Co-IF for β-CAT and mesenchymal markers including PECAM or PDGFRα showed that these cells are negative for these markers (data not shown). We did not observe $\beta\text{-CAT}^{Ser552}$–positive cells in the epithelium. In our model, absence of mesenchymal *Pten* affected lipofibroblast, VSMC, and parabronchial SMC (PSMC) differentiation likely due to increased levels of Ser^{552} β-CAT, a recognized positive regulator of stem cell homeostasis downstream of the AKT pathway.

The pulmonary mesenchyme is the source of many signaling factors, the most important of which is FGF10, which interacts with receptor tyrosine kinases (RTKs). *Fgf10* expression by the mesenchyme is positively regulated by WNT and FGF9 signaling and is negatively regulated by sonic hedgehog (SHH) (2, 4). Deletion of *Fgf10* leads to lung agenesis, suggesting a key role in mediating mesenchymal-epithelial interactions that are necessary for lung morphogenesis (17, 18). FGF10 is the major FGFR2b ligand during the pseudoglandular stage. FGF10 is secreted exclusively by the mesenchyme and acts on the epithelium through FGFR2b.

Because of the increase in $\beta\text{-CAT}^{Ser552}$, *Fgf10* expression was analyzed by in situ hybridization (ISH). *Fgf10* mRNA was increased in mutant lungs compared with controls (Figure 5, B vs. A). qRT-PCR analysis for *Fgf10* confirmed the ISH results (Figure 5I, 2.09 ± 0.48 vs. 1, $P < 0.05$). A downstream pathway activated by FGF10 in the epithelium is β-CAT signaling (3). To examine whether the observed increased FGF10 and increased mesenchymal $\beta\text{-CAT}^{Ser552}$ stimulates β-CAT signaling, we generated triple transgenic mice composed of $Pten^{fl/fl;Dermo\text{-}Cre}$ mice and *Batgal*, the latter a WNT signaling reporter (19), and analyzed the embryos at E15.5 (Figure 5, C–F). β-CAT signaling was increased in lung epithelium and mesenchyme of the $Pten^{fl/fl;Dermo\text{-}Cre}$;*Batgal* lungs compared with controls (Figure 5, D and F vs. C and E).

Mesenchymal Pten inactivation leads to expansion of the distal epithelial progenitor cell domain characterized by ID2 and SPC expression. Since activated β-CAT is recognized as controlling stem cell homeostasis in lung epithelial cells, we performed IF for epithelial markers in E18.5 control and mutant lungs (Figure 6, C–H). Double IF with antibodies to E-CAD and FGFR2 showed increased FGFR2 in E18.5 $Pten^{fl/fl;Dermo\text{-}Cre}$ lungs compared with controls (Figure 6, B vs. A). qRT-PCR confirmed this observation by showing a 4-fold increase of *Fgfr2b* mRNA in mutant lungs (Figure 6I, 4.1 ± 0.3 vs. 1, $P < 0.01$). qRT-PCR showed increased expression for *Fgf9* and *Fgf7,* 2 additional growth factors made by the lung mesothelium/epithelium (*Fgf9*) and by the mesenchyme (*Fgf7*), (Figure 6I, *Fgf9:* 2.6 ± 0.5 vs. 1, $P < 0.05$; *Fgf7*: 5.7 vs. 1 ± 1.6, $P < 0.05$). To validate these results, we also examined the expression of FGF10/FGFR2b downstream and positive regulator targets by qRT-PCR. As expected, compared with the controls, *Wnt2b*, *Spry2*, *Etv4*, *Etv5*, and *Bmp4* were increased, while *Shh*, *Ptch1*, and *Gli1* decreased in the mutant lungs (Figure 6I, *Wnt2b*: 3.03 ± 1.2 vs. 1, NS; *Spry2*: 2.46 ± 0.58 vs. 1, $P < 0.05$; *Etv4*: 1.26 ± 0.15 vs. 1, NS; *Etv5*: 1.56 ± 0.24 vs. 1, $P < 0.05$; *Bmp4*: 1.26 ± 0.06 vs. 1, $P < 0.01$; Figure 6I, *Shh*: 0.6 ± 0.3 vs. 1, $P < 0.05$; *Ptch1*: 0.47 ± 0.1, $P < 0.05$; *Gli1*: 0.5% ± 0.06 vs. 1, $P < 0.01$).

As we observed increased FGF10 activity in the epithelium of the mutant lungs, we investigated whether this change affected epithelial differentiation along the pulmonary proximal and distal domains (20). IHC for SPC, T1α, and CC10 markers for alveolar type 2 (distal domain), alveolar type 1 (distal domain) and Clara cells (proximal domain), respectively, showed an increase of alveolar type 2 (SPC-positive) cells, while the Clara cells (CC10-positive) and type 1 cells (T1α-positive) were unchanged

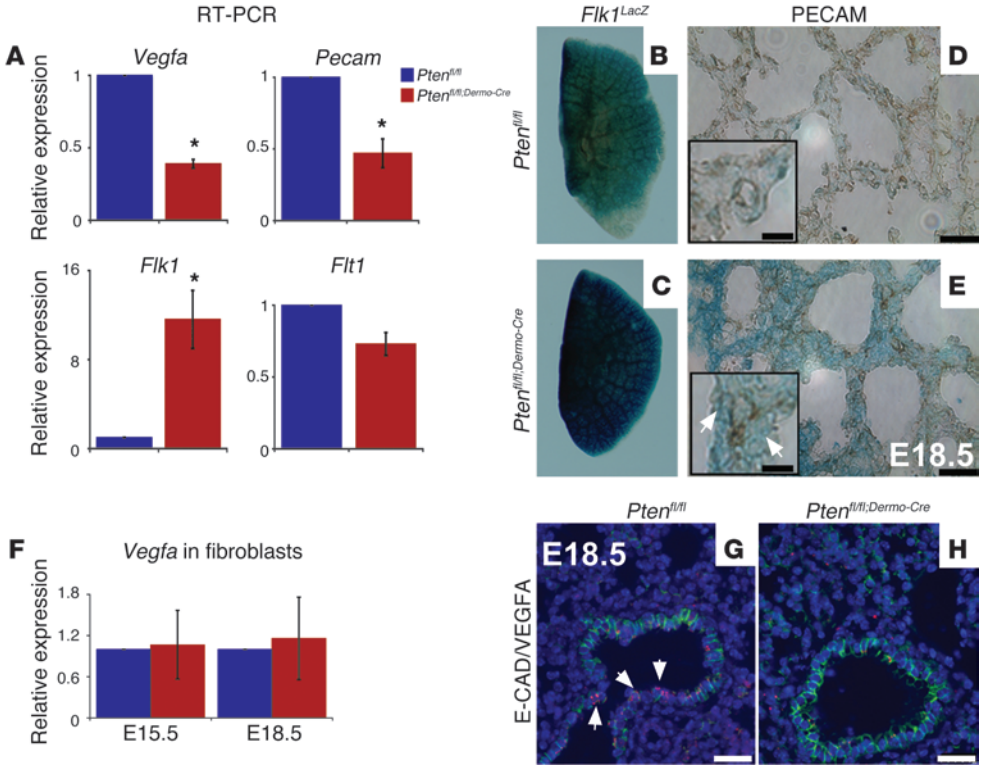

Figure 3
Defect in angioblast differentiation in *Pten*$^{fl/fl;Dermo\text{-}Cre}$ lungs. (**A**) Altered vascular gene expression in E18.5 mutant lungs. qRT-PCR of mRNA using 4 different lungs/group showed decreased *Vegfa*, *Pecam*, and *Flt1* and increased *Flk1*. GAPDH or β-actin served as target reference. *Statistically significant: $P < 0.05$. (**B**–**E**) β-gal staining of E18.5 *Pten*$^{fl/fl}$;*Flk1*$^{LacZ/+}$ and *Pten*$^{fl/fl;Dermo\text{-}Cre}$;*Flk1*$^{LacZ/+}$ lungs showing increased *Flk1*-positive cells, a marker for angioblasts in the mutant lungs. (**B** and **C**) Whole-mount β-gal staining of the left lobe. Increased *Flk1*-positive cells in the mutant lungs compared with control was observed. (**D** and **E**) Double staining showed majority of Flk1-positive cells are PECAM negative. Scale bars: 25 μm (lower magnification), 50 μm (higher magnification) (**B**–**E**). (**F**) qRT-PCR using E15.5 and E18.5 fibroblasts showing no differences in *Vegfa* between control and mutant samples, indicating decreased total *Vegfa* occurs in the epithelium. (**G** and **H**) Immunofluorescence for E-CAD (green) and VEGFA (red) in E18.5 lungs. Note presence of VEGFA in E-CAD–positive cells (white arrows: epithelium) in the control and its absence in the mutant lungs. Scale bars: 25 μm (**G**, **H**).

in the *Pten*$^{fl/fl;Dermo\text{-}Cre}$ lungs compared with *Pten*$^{fl/fl}$ controls (Figure 6, C–H). Western blot analysis demonstrated a statistically significant increase in SPC expression (marker for alveolar type 2 cells) in the mutant compared with controls (Figure 6J, SPC: 0.2 ± 0.003 vs. 0.09 ± 0.003, in arbitrary units, $P < 0.05$). In addition, comparison of CC10 and T1α expression showed no statistical difference between the 2 groups (data not shown). Finally, we performed IHC for TTF1 (NKX2.1), the first transcriptional factor present in the lung during embryogenesis (21), and for ID2, a marker of distal lung progenitor cells (22). The increase in TTF1-positive cells (Figure 6, L vs. K) and ID2/E-CAD–double-positive cells (Figure 6, N vs. M) in the mutant lungs compared with the control confirmed the expansion of the distal domain. Western blot results further confirmed the latter results, showing an increase of TTF1 (0.13 ± 0.006 vs. 0.23 ± 0.006, $P < 0.01$) in the mutants compared with controls (Figure 6J). Overall, these data suggest that the increase in FGF10 signaling in the epithelium, due to *Pten* mesenchymal inactivation, is the likely cause of distal epithelial domain expansion.

Mesenchymal Pten inactivation phenocopies ACD. As the phenotype of the lungs with mesenchymal *Pten* inactivation resembled what has been described in newborn infants as ACD, we examined the hypothesis that the PTEN/PI3K/AKT pathway is activated in the lungs of ACD patients. For this purpose, we performed PTEN and p-AKT IHC on 5 different and independent lung samples from newborn human infants who died with ACD diagnosis and compared these to lungs of newborns who died of causes unrelated to ACD. ACD patients showed a decrease of PTEN staining and a corresponding increase in p-AKT–positive cells compared with lungs from control patients. While PTEN staining was readily detectable (Figure 7, B vs. A), the number of p-AKT–positive cells was limited in the control lungs (Figure 7, D vs. C). Statistical analysis showed an increase in the percentage of p-AKT–positive cells in the ACD lungs compared with controls (Figure 7F, 1.4 ± 0.4 vs. 0.07 ± 0.05, $P < 0.05$).

ACD has been associated with mutations in Forkhead box protein F1 (*FOXF1*) in humans and heterozygous *Foxf1* and *Foxc2* loss of function in mice (23, 24). Accordingly, *Foxf1* and *Foxc2* mRNA were measured by qRT-PCR. We found decreased expression of both genes in mutant compared with control lungs (Figure 7E, *Foxf1*: 0.59 ± 0.015 vs. 1, $P < 0.01$; *Foxc2*: 0.57 ± 0.13 vs. 1, $P < 0.05$). These data support the involvement of the PTEN/PI3K/AKT pathway in the pathogenesis of ACD and justify further analysis of this pathway in our newly described mouse model of a lethal human congenital lung disease.

Discussion

Mesodermal Pten inactivation disrupts lung vasculogenesis. A well-organized and functional capillary network is essential for air-blood gas exchange and therefore for oxygenation of tissues and organs. Impaired development of the vascular capillary network in the lung can cause life-threatening deficiencies in pulmonary function present in neonatal diseases such as BPD and ACD (25, 26).

The results of the present work show that inactivation of *Pten* in the mesodermal lineages that contribute to lung morphogenesis disrupts normal capillary plexus formation as well as mesenchymal and epithelial differentiation.

The role of PTEN in mesodermal lineage formation during lung development had not been hitherto adequately examined. *Pten*

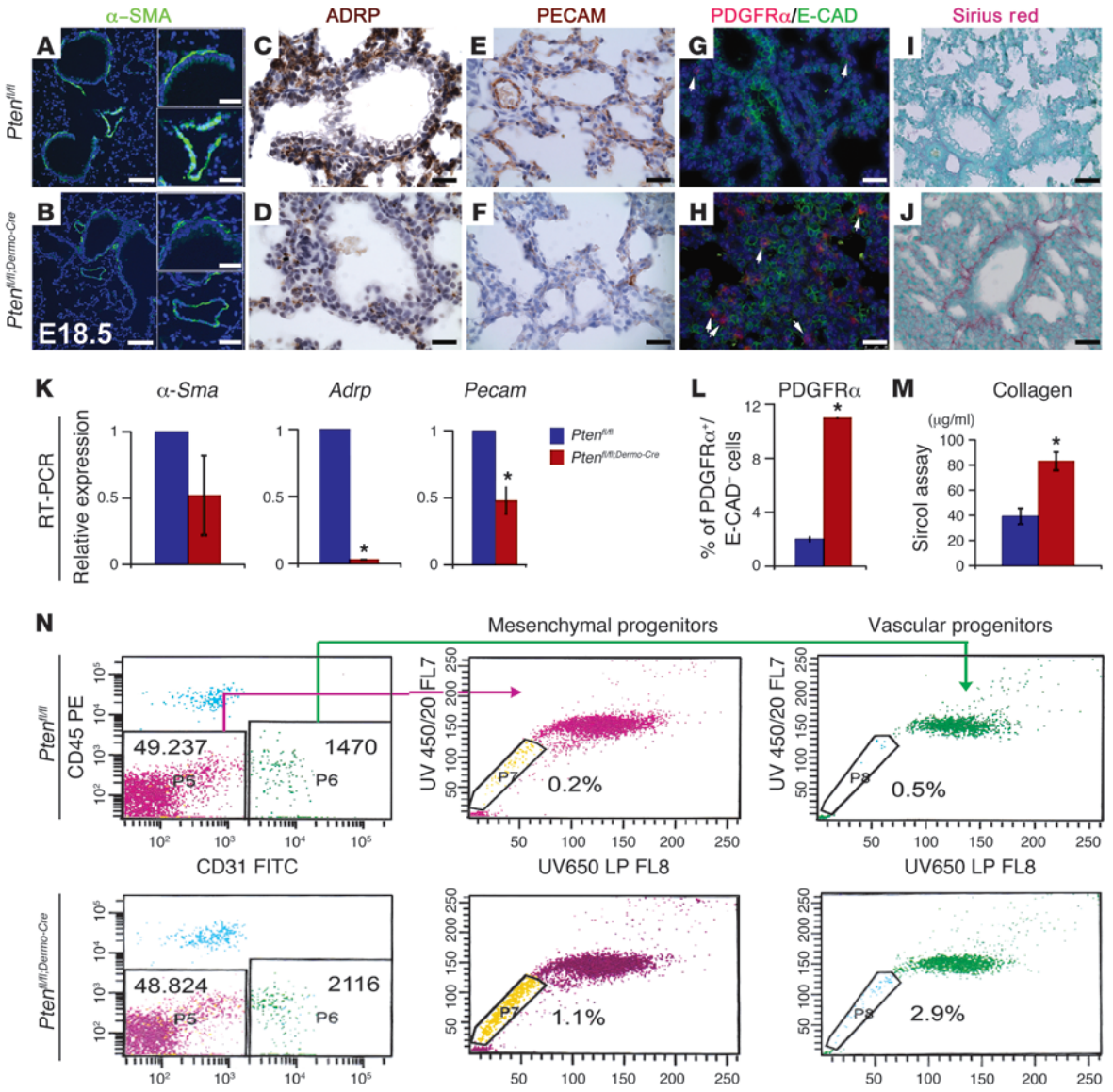

Figure 4

Arrested mesenchymal cell differentiation in *Pten*$^{fl/fl;Dermo\text{-}Cre}$ lungs. (**A**–**F**) IHC for α-SMA, ADRP, and PECAM in E18.5 lungs showing reduced expression in mutant (**B**, **D**, and **F**) compared with control (**A**, **C**, and **E**) lungs. $n = 4$ lungs per group. Scale bars: 50 μm (lower magnification), 25 μm (higher magnification) (**A** and **B**). (**G** and **H**) IF for PDGFRα (fibroblast marker) and E-CAD (epithelial marker) showing increased PDGFRα; E-CAD$^-$ cells (white arrows) in mutant lungs. (**I** and **J**) Sirius red staining showing increased collagen in *Pten*$^{fl/fl;Dermo\text{-}Cre}$ lungs. Scale bars: 25 μm (**C**–**J**).(**K**) qRT-PCR showing decreased mesenchymal differentiation markers, α-*Sma*, *Adrp* in mutant fibroblasts and *Pecam* in mutant total lung. *Statistically significant: *Adrp*, $P \le 0.01$; *Pecam*, $P \le 0.01$; number of *Pdgfra*-positive/*E-cadherin*–negative cells, $P \le 0.01$; collagen, $P \le 0.01$. (**L**) Quantification of PDGFRα and E-CAD$^-$ cells. (**M**) Quantification of collagen 1. (**N**) *Pten* deficiency induced increased embryonic mesenchymal progenitor side populations (E-SP). Representative flow cytometric profiles of side population in E17.5 lungs. Upper panels, WT cells; lower panels, mutant cells. Side populations were identified by Hoechst 33342, CD45, and CD31 antibodies. The percentages of side populations (boxed areas) in total lung are indicated in each panel. E-SP$^-$CD45$^-$CD31$^-$ and E-SP$^-$CD45$^-$CD31$^+$ cells identify smooth muscle and vascular progenitors in side populations, respectively. Data represent a pool of 14 lungs/group.

was previously shown to be important in regulating proliferation of endothelial cells (10). Endothelial-specific inactivation of *Pten* using the *Tie2-Cre* driver mice led to early embryonic lethality due to fatal vascular remodeling defects secondary to an impaired recruitment of VSMCs. Hamada and colleagues (10) showed also that the absence of PTEN in endothelial cells causes hypersensitivity to VEGFs, resulting in enhanced angiogenesis and bleeding due to a failure in vascular remodeling. Deleris et al. (11) found that PTEN is also expressed and active in VSMCs controlling the level of PIP3 and therefore potentially controlling VSMC proliferation. Another report (27) showed that absence of PTEN in VSMCs leads to vascular remodeling and increased progenitor cell recruitment. However, to date, the specific deletion of *Pten* in lung mesenchyme during development has not been reported.

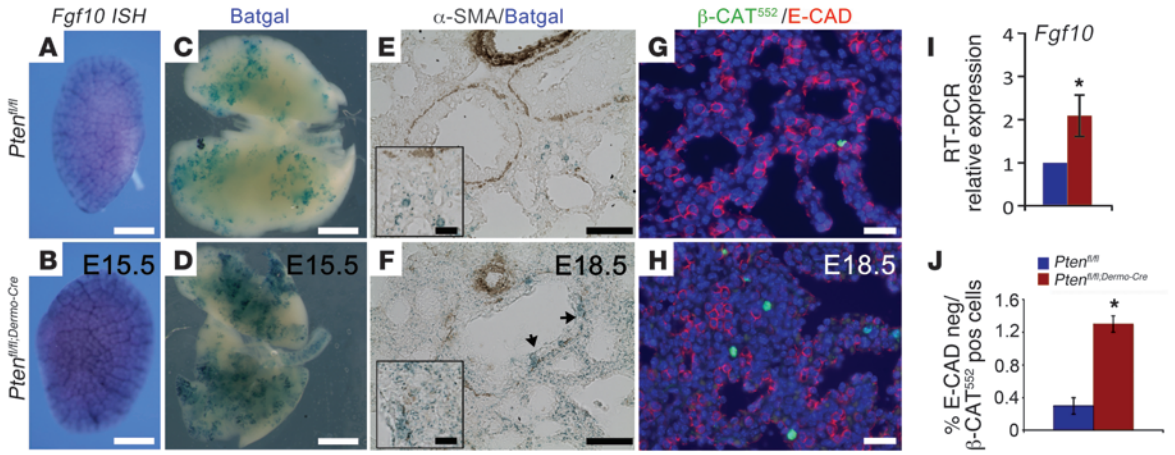

Figure 5

Increase in mesenchymal progenitor cells is due to increased β-CAT and FGF10 signaling. (**A** and **B**) Whole-mount ISH for *Fgf10* at E15.5 showing increased expression in the mutant lungs. (**C**–**F**) β-gal staining in *Batgal* background. Increased WNT signaling in mutant lungs compared with controls. (**C** and **D**) Whole-mount images of left lobes. (**E** and **F**) Double α-SMA, β-gal staining showed increased WNT signaling in epithelial and mesenchymal (not α-SMA–positive) cells. (**G** and **H**) Double staining for E-CAD/Ser^{552} β-CAT showing increased WNT signaling in mesenchymal cells. Scale bars: 50 μm (lower magnification), 25 μm (higher magnification) (**E** and **F**); 25 μm (**G** and **H**).(**I**) qRT-PCR for *Fgf10* showing increased *Fgf10* in mutant lungs versus control. (**J**) Statistical analysis of β-CAT^{Ser552}–positive/E-CAD–negative cells in mutant versus control lungs, n = 3/each group. *Statistically significant: *Fgf10*, $P \leq 0.05$; β-CAT^{Ser552}–positive/E-CAD–negative cells, $P \leq 0.01$.

In the present work, we used the *Dermo1-Cre* driver line to inactivate *Pten* from the onset of lung morphogenesis (i.e., E9.5) in all mesodermally derived cells (refs. 12, 28, and Supplemental Figure 1G) except for endothelial progenitors. The resulting mutant mice exhibited perinatal lethality that was largely due to vascular defects and mesenchymal hypercellularity. The newborn mice were clearly hypoxemic and could not oxygenate their blood. Detailed examination of their lungs revealed decreased capillary formation, but more importantly, misalignment of the existing capillary network with the airways, due also to the increased number of mesenchymal cells in the parenchyma. Interestingly, our genetic manipulation, which enabled the embryos to survive until birth, is significantly different from the one resulting from endothelial-specific deletion of *Pten* (10). Thus, the use of the *Dermo1-Cre* driver line to delete *Pten* in all mesodermally derived cells except for endothelial cells provides new insight into the key role played by PTEN in mesodermal lineage formation.

To investigate the underlying mechanisms for the observed vascular defects in *Pten*$^{fl/fl;Dermo\text{-}Cre}$ mutants, we measured a number of relevant parameters. *Vegfa* was markedly reduced in the mutant lungs at E18.5. *Vegfa* is first expressed in the distal subepithelial mesenchyme, but begins to be expressed also in the epithelium at E14.5 (1). Thereafter, *Vegfa* becomes progressively restricted to the epithelium (1). It is therefore likely that the main source of *Vegfa,* whose secretion is decreased in our mutants, is the epithelium. Interestingly, the decrease in VEGFA occurs in spite of increased FGF10 signaling to the epithelium, which we had previously shown to be a positive regulator of *Vegfa*, using *Fgf10* hypomorphic mice (3). However, in these mutants, this decrease is likely the consequence of reduced epithelial cell numbers rather than being caused by a direct transcriptional regulation of *Vegfa* by FGF10. In support of this observation, the decrease in *TTF1* expression (marker of lung epithelium) in the lungs of *Fgf10* hypomorphic embryos was also apparent within the same range as was observed for *Vegfa* (3). The change in *Vegfa* therefore is indirect and may reflect changes in the epithelial/mesenchymal ratio, which was drastically changed in favor of the mesenchyme in *Pten*$^{fl/fl;Dermo\text{-}Cre}$ lungs (higher FGF10 signal leads to only modest epithelial progenitor cell increase, whereas mesodermal *Pten* inactivation causes a marked increase in mesenchymal proliferation). This, in turn, will automatically lead to a global decrease in *Vegfa* expression in the lung. Reduced VEGFA will undoubtedly cause corresponding defects in vascular formation. In addition, SHH and FGF9 are reported to be critical for vascular development (1). Therefore, as *Shh* is decreased, vascular (endothelial) development is also expected to be impaired in *Pten*$^{fl/fl;Dermo\text{-}Cre}$ lungs.

Interestingly, the lack of differentiation in the epithelial compartment was associated with increased angioblasts in the mesenchyme. This was supported by the increase in *Flk1* (marker of vascular progenitors), but also by concomitant decrease in *Flt1* and *Pecam* (both markers of differentiated endothelial cells) mRNAs. As previously demonstrated, absence of *Flt1* leads to disorganized angiogenesis due to the role of this receptor in vascular commitment (29). Moreover, PTEN may not be necessary for differentiation of angioblasts from the ventral mesoderm and for their migration within the lung, as has been shown previously (10). Accordingly, we observed that the absence of PTEN did not affect the formation of the major vessels or the angioblast population. Nevertheless, our studies identified an important role for mesenchymal *Pten* in the differentiation of angioblasts to endothelial cells. As *Pten* is not deleted in endothelial cells, this role is likely indirect, being an outcome of alterations in mesenchymal-endothelial or mesenchymal-epithelial-endothelial crosstalk mediated by as yet unknown signaling molecules.

In the course of this study, we also noticed that PTEN in the lung mesenchymal cells was present both in the cytoplasm and in the nuclei, while in the epithelium, PTEN was confined only to the cytoplasm. A recent report investigating the role of PTEN

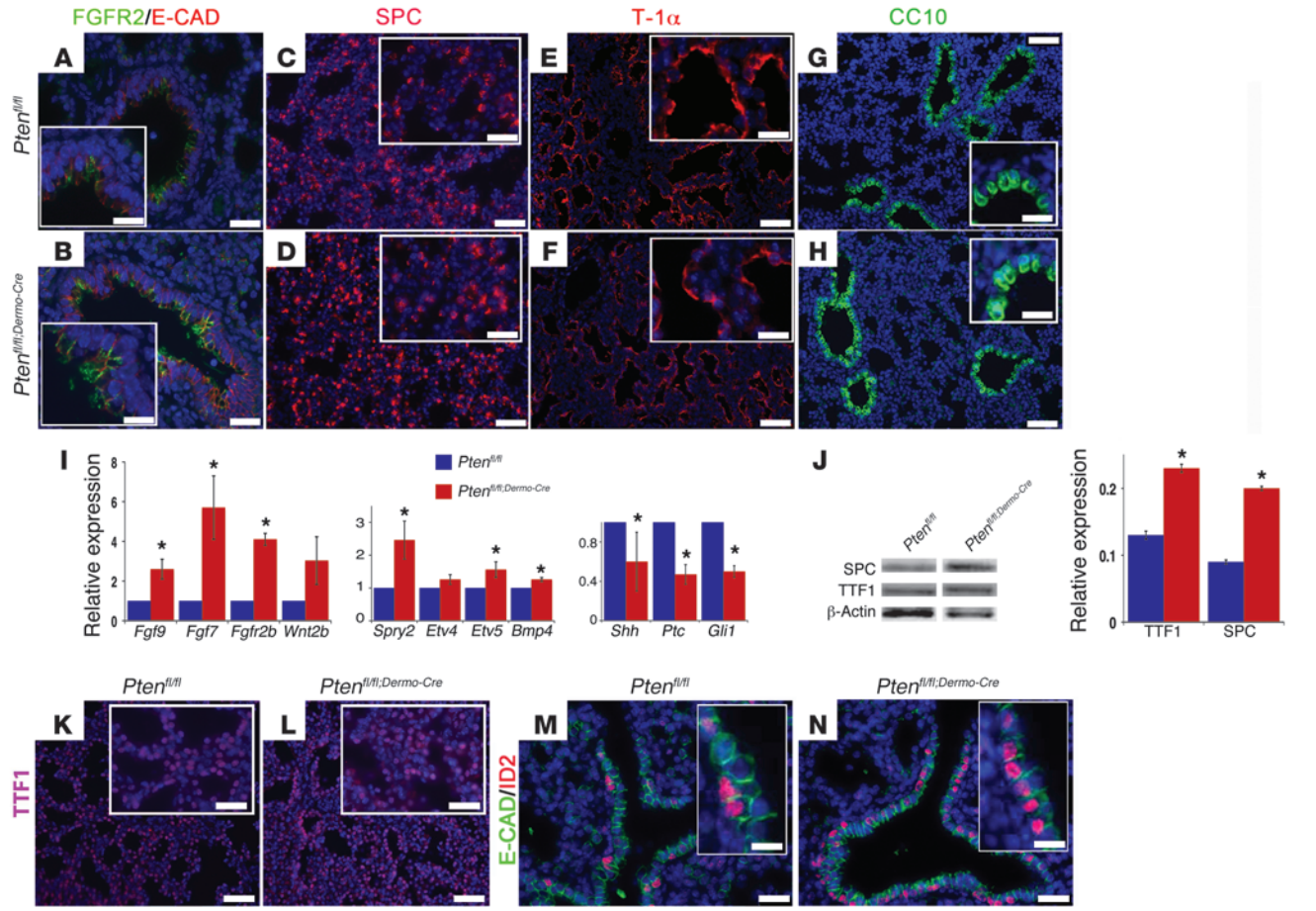

Figure 6

Analysis of epithelial differentiation suggests increased FGF signaling. (**A**–**H**) IHC in E18.5 lungs showing increased SPC and FGFR2 in epithelium of mutant lungs. CC10 and T1α staining showed no differences. (**I**) qRT-PCR for *Fgfr2b*, *Fgf9*, *Fgf7*, *Wnt2b*, *Spry2*, *Etv4*, *Etv5*, *Bmp4*, *Shh*, *Ptch1*, and *Gli1* showed increased FGF10/FGFR2b signaling in epithelium of the *Pten* cKO lungs compared with the WT. (**J**) Western blot for epithelial markers showed increased progenitor markers (SPC and TTF1) in the *Pten*$^{fl/fl;Dermo\text{-}Cre}$ lungs. Data represent 5 lungs/group. *Statistically significant: *Fgf9*, $P \le 0.05$; *Fgf7*, $P \le 0.05$; *Fgfr2b*, $P \le 0.01$; *Spry2*, $P \le 0.05$; *Etv5*, $P \le 0.05$; *Bmp4*, $P \le 0.01$; *Shh*, $P \le 0.05$; *Ptch1*, $P \le 0.05$; *Gli1*, $P \le 0.01$. (**K** and **N**) IHC for TTF1 and E-CAD/ID2 in E18.5 control and mutant lungs. TTF1 and E-CAD/ID2 double-positive cells, markers of distal epithelial cells, were increased in the mutant lungs. Scale bars: 25 μm (lower magnification), 10 μm (higher magnification) (**A**, **B**, **M**, **N**); 50 μm (lower magnification), 30 μm (higher magnification) (**C**, **D**, **K**, **L**); 50 μm (lower magnification), 25 μm (higher magnification) (**E**–**H**).

in cancer cells showed that nuclear-localized PTEN interacts with APC/C (anaphase promoting complex) and promotes its association with Fizzy-related protein 1 (FZR1), thereby enhancing tumor-suppressive activity of the APC/C-FZR1 complex in a phosphatase-independent manner (30). In this way, both proliferation and senescence are affected by reduction of APC/C activity upon *Pten* loss. Whether the lack of PTEN in the nuclei or in the cytoplasm of mesenchymal cells is responsible for some aspect of the phenotype observed in *Pten*$^{fl/fl;Dermo\text{-}Cre}$ lungs remains to be clarified by future studies.

PTEN controls lung mesenchyme differentiation. The mesenchyme is essential during lung development, as it contains the progenitors for several mesenchymal cell types that include the PSMCs, the VSMCs, the lipofibroblast, the alveolar myofibroblasts, and the stromal fibroblasts (31, 32). The proper generation of these cells relies on the controlled amplification of progenitors followed by the exit of these cells from the cell cycle and their timely differentiation into appropriate progeny (2). Several studies (9, 33) have shown that epithelial inactivation of *Pten* in the lung leads to an increase in epithelial progenitor cells and impaired epithelial cell differentiation. In our model, absence of mesenchymal *Pten* affected lipofibroblast, VSMC, and PSMC differentiation, likely via an increase in β-CAT Ser^{552}–mediated WNT signaling, a recognized regulator of epithelial stem cell homeostasis. Indeed, we have previously shown that mesenchymal-specific deletion of β-CAT results in lack of amplification and premature differentiation of PSMC progenitor cells (2). Moreover, we have recently shown that reactivation of Wnt signaling in mature PSMC after airway epithelial injury results in their dedifferentiation and adoption of a PSMC progenitor-like state and reexpression of *Fgf10* (34). Interestingly, in contrast to our findings, others have reported increased SMC differentiation associated with increased WNT signaling (35). One difference is that in the latter study, SMC-specific targeting was employed, while in our study, *Dermo1-Cre* driver line targeted the mesenchymal progenitor cells. In addition, treatment of lung explants in the pseudoglandular stage with LiCl to increase Wnt

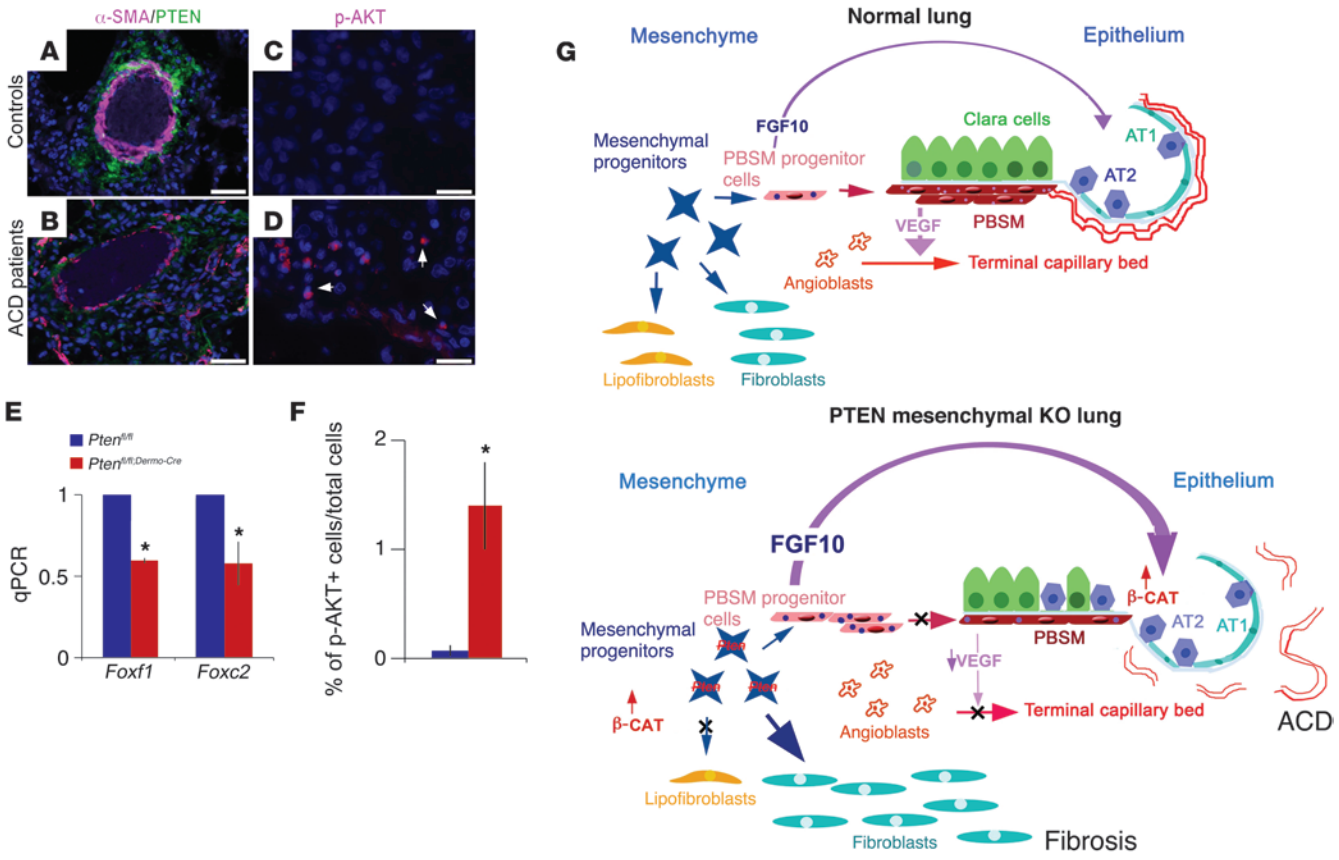

Figure 7

Human newborn ACD lungs display decreased PTEN and increased p-AKT. (**A** and **B**) IHC for PTEN in human ACD and control lungs showing decreased PTEN in the ACD patients. (**C** and **D**) IF for p-AKT showing increased p-AKT–positive cells. (**E**) qRT-PCR using mRNA from *Pten*$^{fl/fl}$ and *Pten*$^{fl/fl;Dermo\text{-}Cre}$ lungs showed decreased *Foxf1* and *Foxc2* in the mutant lungs. (**F**) Statistical analysis showed increased p-AKT–positive cell percentage in ACD lungs. *Statistically significant: *Foxf1*, $P \leq 0.01$; *Foxc2*, $P \leq 0.05$. (**G**) Cellular and molecular mechanisms resulting from mesenchymal PTEN deletion in the lung. Scale bars: 40 μm (**A** and **B**); 20 μm (**C** and **D**).

signaling in both epithelium and the mesenchyme was associated with increased α-SMA around bronchi and blood vessels (35). Preliminary data from our group show that after *Dermo1-Cre* deletion of the negative regulator of WNT signaling, adenomatous polyposis coli (leading to increased β-CAT signaling) differentiation of α-SMA cells was blocked (P. Minoo et al., unpublished data). These data are consistent with our findings in the present manuscript. Thus, lack of β-CAT in the mesenchyme led to premature differentiation of PSMC and lack of amplification of the progenitors, while increased WNT signaling blocked differentiation and increased mesenchymal progenitors. Finally, *Pten* deletion during embryonic stages led to increased collagen production. This could occur either by induction of collagen expression in mesenchymal progenitors or by promotion of fibroblast differentiation. Interestingly, several studies have reported decrease or absence of PTEN in fibrotic foci in idiopathic pulmonary fibrosis (IPF) (36).

Mesodermal Pten inactivation affects epithelial differentiation via increased FGF10 and WNT signaling. Epithelial-mesenchymal interactions mediated via key signaling factors during lung development are critical for proper patterning of the epithelium and mesenchyme along the proximal-distal axis. The mesenchyme is the source of important signaling factors, such as FGF10, required for airway epithelial development and branching. Also, the epithelium produces signaling molecules essential for mesenchymal differentiation and proliferation, such as bone morphogenetic protein 4 (BMP4), SHH (18, 37, 38), and FGF9 (1). The observations in this study showed that mesodermal *Pten* inactivation caused increased *Fgf9*, *Fgf10*, and *Fgf7* expression and decreased expression of *Shh*, *Ptch1*, and *Gli1*. We further found that increase in FGF10 caused increased FGFR2b signaling, supported by upregulation of FGF10 downstream targets *Fgfr2b*, *Bmp4*, and *Spry2*. Such changes in *Pten*$^{fl/fl;Dermo\text{-}Cre}$ lungs would undoubtedly have an impact on lung development and cell differentiation. Thus, mesenchymal-specific inactivation of *Pten* led to arrested differentiation of mesoderm-derived cells. Concomitantly, we observed an increase in the number of SMC progenitors, which include the *Fgf10*-positive cells. The latter have been described as giving rise to PSMCs. The increased number of *Fgf10*-expressing cells is likely responsible for increased expression of FGF10 downstream targets *Fgfr2b*, *Bmp4*, and *Spry2* in the mutant lungs. These cells proliferate and give rise to an increased number of distal SPC-positive cells. IHC analysis for ID2, a distal cell marker, suggested alterations in proximal-distal differentiation of epithelial cells; increased numbers of ID2-positive cells were found to be localized proximally in the mutant lung. Interestingly, we did not detect any defect in epithelial differentiation in the proximal

lung; CC10 and T1α staining indicated a normal pool of Clara and type 1 cells in both mutants and control lungs. Therefore, absence of PTEN in the mesenchyme leads to the expansion of the pool of distal epithelial progenitor cells likely secondary to increased FGF10/FGFR2b signaling in the epithelium.

Mesodermal Pten inactivation leads to ACD-like phenotype. Our observations suggested vascular similarities in phenotype between $Pten^{fl/fl;Dermo\text{-}Cre}$ lungs and the lungs of human neonates with ACD. FGF9 and SHH pathways were previously shown to be important for vasculogenesis, and disruption of their function leads to ACD-like phenotypes (1). Consistent with the latter findings,we found alterations in both FGF9 and SHH pathways in $Pten^{fl/fl;Dermo\text{-}Cre}$ lungs. qRT-PCR revealed increased *Fgf9* mRNA, while *Shh* and its downstream targets, *Ptch1* and *Gli1*, were decreased in the mutant lungs (Figure 6I). Thus, both the vascular phenotype and the molecular alterations in $Pten^{fl/fl;Dermo\text{-}Cre}$ lungs are consistent with the features associated with human ACD. Furthermore, a significant decrease in *Foxf1* and *Foxc2* mRNAs (Figure 7E) was also documented in the $Pten^{fl/fl;Dermo\text{-}Cre}$ lungs, also consistent with previous findings in human and murine ACD phenotype (23, 24). Finally, to directly ascertain the relevance of our findings in human tissues, we conducted IHC for PTEN and p-AKT in 5 independent human lung samples from ACD patients and newborns who died of causes other than ACD. The absence of PTEN staining and the increase in p-AKT–positive cells in ACD lungs demonstrated that the PI3K/AKT pathway is activated and that loss of PTEN may be relevant to this activation. It has been reported that *Foxf1* expression is directly inhibited by AKT in liver myofibroblasts (39). Therefore, it is possible that a similar situation occurs also in the lung where *Foxf1* could be a direct transcriptional target for PTEN signaling in the lung mesenchyme through AKT activation. Whether loss of PTEN can be recognized as primum movens in the pathogenesis of ACD and whether activation of PTEN can be used as a therapeutic target remains to be determined.

In conclusion, mesodermal-specific inactivation of *Pten* by *Dermo1-Cre* leads to a phenotype resembling ACD, a dramatic neonatal disease with 100% mortality at birth. The cellular mechanisms underlying the phenotype are connected with an increase in mesenchymal progenitor cells and a reduced differentiation of these cells into PSMCs and lipofibroblasts. This also leads indirectly to an increase in the angioblast pool as well as defective differentiation of these cells into endothelial cells. We propose a model whereby increased FGF10-expressing PSMC progenitor cells activate the FGF10/FGFR2b pathway in the epithelium, leading to an expansion of the distal progenitor pools containing ID2-positive cells. Lack of epithelial differentiation also leads to decreased *Vegfa* during early embryonic stages that in turn causes defects in capillary development around the primitive alveoli and, therefore, a lack of oxygenation at birth, with subsequent perinatal lethality. Finally, blocked differentiation of mesenchymal progenitors to SMC and lipofibroblasts drives progenitor cells toward an alternative fibroblast phenotype, leading to increased collagen production (Figure 7G).

Methods

Transgenic mice. $Pten^{fl/fl}$ (C57BL/6 background; stock no. 006440), $Flk1^{LacZ/+}$ (stock no. 002938), *Dermo1-Cre* (stock no. 008712), and *Batgal* (stock no. 005317) mice were from Jackson Laboratory. *Pten* knockouts were obtained by mating $Pten^{fl/fl}$ females with *Dermo1-Cre* male mice (C57BL/6 background) for 2 generations to obtain *Dermo1-Cre;* $Pten^{fl/fl}$ (heretofore $Pten^{fl/fl;Dermo\text{-}Cre}$) and *Dermo1-cre;*$Pten^{fl/+}$ (heretofore $Pten^{fl/+;Dermo\text{-}Cre}$) on a C57BL/6 background. $Pten^{fl/fl}$ mice were used as control. Genotyping of the *Dermo1-Cre* mice containing $Pten^{fl}$, $Pten^{\Delta}$, and $Pten^{WT}$ alleles was as previously described (12, 40).

Blood saturation. Heart rate and transcutaneous oxygen saturation were monitored every 10 seconds for 1 minute in newborn mice via a pulse oximeter (MouseOx; STARR Life Sciences Corporation) by placing noninvasive sensors on the back of the newborn mice.

Tissue collection. Lungs from embryos were collected at E15.5 and E18.5 and fixed overnight, dehydrated through increasing ethanol concentrations, embedded in paraffin, and prepared as 5-μm sections.

Fibroblast isolation. E18.5 lungs (6 controls and 6 mutants) were mechanically disrupted and incubated at 37°C with 1:1 Trypsin 0.025%/EDTA: DMEM/F12. Dissociated cells were passed through a 19.5- to 27-gauge needle, incubated in DMEM/F12 with 10% FBS (2 hours), and washed 10 times with DMEM/F12. Adherent fibroblasts were grown for 24 hours, detached by scraping, and centrifuged (at 1,700 *g* for 5 minutes). Cell pellets were stored at –80°C.

Statistics. Data were presented as means ± SEM unless stated otherwise. The data were statistically analyzed using 2-tailed Student's *t* tests to compare the 2 groups. $P < 0.05$ was considered significant.

Study approval. All animal experiments were approved by the University of Southern California Animal Use and Care Committee. Post mortem unidentified human ACD tissue was contributed by P. Sen and C. Langston (Baylor College of Medicine, Houston, Texas, USA) (IRB number, H-8712).

Acknowledgments

This work was supported by NIH HL56594 (to P. Minoo), HL086322 (to S. Bellusci), HL074832 (to S. Bellusci), the Excellence Cluster Cardio-Pulmonary System, LOEWE (to S. Bellusci), HL092967 (to S. De Langhe), the Hastings Foundation (to P. Minoo), the CIRM Clinical Fellowship (to C. Tiozzo and G. Carraro), NIH K12-HD-052954 (to B. Chan), and the American Lung Association as well as the American Heart Association (to D.A. Alam). P. Minoo is Hastings Professor of Pediatrics. S. Bellusci holds the chair of Lung Matrix Remodelling at Justus Liebig University. Z. Borok is Edgington Chair in Medicine. The authors also thank the ACD Association and P. Sen and C. Langston (Baylor College of Medicine) for providing human ACD lung samples. We thank Hiroyuki Shimada (Children's Hospital, Los Angeles) for discussion and technical support, Esteban Fernandez for help with tridimensional reconstruction of lung vasculature, and Clarence Wigfall for help with the processing of the videos. C. Tiozzo acknowledges C. Fagan and L. Barrow.

Received for publication October 7, 2011, and accepted in revised form August 2, 2012.

Address correspondence to: Parviz Minoo, General Lab Building, Women's and Children's Hospital, 1801 E. Marengo St., Los Angeles, California 90033, USA. Phone: 323.226.4340; Fax: 323.226.5049; E-mail: minoo@usc.edu. Or to: Saverio Bellusci, Department of Internal Medicine II, University of Giessen Lung Center, Excellence Cluster in Cardio-Pulmonary Systems, Aulweg 130, Giessen 35392, Germany. Phone: 49.0.641.99.46.730; Fax: 49.0.641.99.46.739; E-mail: Saverio.Bellusci@innere.med.uni-giessen.de.

Caterina Tiozzo's present address is: Nassau University Medical Center, Pediatrics Department, East Meadow, New York, USA.

1. White AC, Lavine KJ, Ornitz DM. FGF9 and SHH regulate mesenchymal Vegfa expression and development of the pulmonary capillary network. *Development*. 2007;134(20):3743–3752.
2. De Langhe SP, et al. Formation and differentiation of multiple mesenchymal lineages during lung development is regulated by beta-catenin signaling. *PLoS One*. 2008;3(1):e1516.
3. Ramasamy SK, et al. Fgf10 dosage is critical for the amplification of epithelial cell progenitors and for the formation of multiple mesenchymal lineages during lung development. *Dev Biol*. 2007;307(2):237–247.
4. Del Moral PM, et al. VEGF-A signaling through Flk-1 is a critical facilitator of early embryonic lung epithelial to endothelial crosstalk and branching morphogenesis. *Dev Biol*. 2006;290(1):177–188.
5. Stenmark KR, Abman SH. Lung vascular development: implications for the pathogenesis of bronchopulmonary dysplasia. *Annu Rev Physiol*. 2005;67:623–661.
6. Ng PC, Lewindon PJ, Siu YK, To KF, Wong W. Congenital misalignment of pulmonary vessels: an unusual syndrome associated with PPHN. *Acta Paediatr*. 1995;84(3):349–353.
7. Cho KW, et al. ERK activation is involved in tooth development via FGF10 signaling. *J Exp Zool B Mol Dev Evol*. 2009;312(8):901–911.
8. Stiles B, Groszer M, Wang S, Jiao J, Wu H. PTENless means more. *Dev Biol*. 2004;273(2):175–184.
9. Tiozzo C, et al. Deletion of Pten expands lung epithelial progenitor pools and confers resistance to airway injury. *Am J Respir Crit Care Med*. 2009; 180(8):701–712.
10. Hamada K, et al. The PTEN/PI3K pathway governs normal vascular development and tumor angiogenesis. *Genes Dev*. 2005;19(17):2054–2065.
11. Deleris P, et al. SHIP-2 and PTEN are expressed and active in vascular smooth muscle cell nuclei, but only SHIP-2 is associated with nuclear speckles. *J Biol Chem*. 2003;278(40):38884–38891.
12. Yu K, et al. Conditional inactivation of FGF receptor 2 reveals an essential role for FGF signaling in the regulation of osteoblast function and bone growth. *Development*. 2003;130(13):3063–3074.
13. Parera MC, et al. Distal angiogenesis: a new concept for lung vascular morphogenesis. *Am J Physiol Lung Cell Mol Physiol*. 2005;288(1):L141–L149.
14. Shalaby F, et al. Failure of blood-island formation and vasculogenesis in Flk-1-deficient mice. *Nature*. 1995;376(6535):62–66.
15. Summer R, Kotton DN, Liang S, Fitzsimmons K, Sun X, Fine A. Embryonic lung side population cells are hematopoietic and vascular precursors. *Am J Respir Cell Mol Biol*. 2005;33(1):32–40.
16. He L, et al. Co-existence of high levels of the PTEN protein with enhanced Akt activation in renal cell carcinoma. *Biochim Biophys Acta*. 2007; 1772(10):1134–1142.
17. Sekine K, et al. Fgf10 is essential for limb and lung formation. *Nat Genet*. 1999;21(1):138–141.
18. Bellusci S, Grindley J, Emoto H, Itoh N, Hogan BL. Fibroblast growth factor 10 (FGF10) and branching morphogenesis in the embryonic mouse lung. *Development*. 1997;124(23):4867–4878.
19. Maretto S, et al. Mapping Wnt/beta-catenin signaling during mouse development and in colorectal tumors. *Proc Natl Acad Sci U S A*. 2003;100(6):3299–3304.
20. Nyeng P, Norgaard GA, Kobberup S, Jensen J. FGF10 maintains distal lung bud epithelium and excessive signaling leads to progenitor state arrest, distalization, and goblet cell metaplasia. *BMC Dev Biol*. 2008;8:2.
21. Minoo P, Su G, Drum H, Bringas P, Kimura S. Defects in tracheoesophageal and lung morphogenesis in Nkx2.1(–/–) mouse embryos. *Dev Biol*. 1999;209(1):60–71.
22. Rawlins EL, Clark CP, Xue Y, Hogan BL. The Id2+ distal tip lung epithelium contains individual multipotent embryonic progenitor cells. *Development*. 2009;136(22):3741–3745.
23. Stankiewicz P, et al. Genomic and genic deletions of the FOX gene cluster on 16q24.1 and inactivating mutations of FOXF1 cause alveolar capillary dysplasia and other malformations. *Am J Hum Genet*. 2009;84(6):780–791.
24. Yu S, Shao L, Kilbride H, Zwick DL. Haploinsufficiencies of FOXF1 and FOXC2 genes associated with lethal alveolar capillary dysplasia and congenital heart disease. *Am J Med Genet A*. 2010;152A(5):1257–1262.
25. Coalson JJ. Pathology of bronchopulmonary dysplasia. *Semin Perinatol*. 2006;30(4):179–184.
26. deMello DE. Pulmonary pathology. *Semin Neonatol*. 2004;9(4):311–329.
27. Nemenoff RA, et al. Targeted deletion of PTEN in smooth muscle cells results in vascular remodeling and recruitment of progenitor cells through induction of stromal cell-derived factor-1alpha. *Circ Res*. 2008;102(9):1036–1045.
28. Morimoto M, Liu Z, Cheng HT, Winters N, Bader D, Kopan R. Canonical Notch signaling in the developing lung is required for determination of arterial smooth muscle cells and selection of Clara versus ciliated cell fate. *J Cell Sci*. 2010; 123(pt 2):213–224.
29. Fong GH, Zhang L, Bryce DM, Peng J. Increased hemangioblast commitment, not vascular disorganization, is the primary defect in flt-1 knock-out mice. *Development*. 1999;126(13):3015–3025.
30. Song MS, et al. Nuclear PTEN regulates the APC-CDH1 tumor-suppressive complex in a phosphatase-independent manner. *Cell*. 2011;144(2):187–199.
31. Mailleux AA, et al. Fgf10 expression identifies parabronchial smooth muscle cell progenitors and is required for their entry into the smooth muscle cell lineage. *Development*. 2005;132(9):2157–2166.
32. Gebb SA, Shannon JM. Tissue interactions mediate early events in pulmonary vasculogenesis. *Dev Dyn*. 2000;217(2):159–169.
33. Yanagi S, et al. Pten controls lung morphogenesis, bronchioalveolar stem cells, and onset of lung adenocarcinomas in mice. *J Clin Invest*. 2007; 117(10):2929–2940.
34. Volckaert T, et al. Parabronchial smooth muscle constitutes an airway epithelial stem cell niche in the mouse lung after injury. *J Clin Invest*. 2011; 121(11):4409–4419.
35. Cohen ED, Ihida-Stansbury K, Lu MM, Panettieri RA, Jones PL, Morrisey EE. Wnt signaling regulates smooth muscle precursor development in the mouse lung via a tenascin C/PDGFR pathway. *J Clin Invest*. 2009;119(9):2538–2549.
36. White ES, et al. Negative regulation of myofibroblast differentiation by PTEN (Phosphatase and Tensin Homolog Deleted on chromosome 10). *Am J Respir Crit Care Med*. 2006;173(1):112–121.
37. Litingtung Y, Lei L, Westphal H, Chiang C. Sonic hedgehog is essential to foregut development. *Nat Genet*. 1998;20(1):58–61.
38. Pepicelli CV, Lewis PM, McMahon AP. Sonic hedgehog regulates branching morphogenesis in the mammalian lung. *Curr Biol*. 1998;8(19):1083–1086.
39. Godichaud S, et al. The grape-derived polyphenol resveratrol differentially affects epidermal and platelet-derived growth factor signaling in human liver myofibroblasts. *Int J Biochem Cell Biol*. 2006;38(4):629–637.
40. Lesche R, et al. Cre/loxP-mediated inactivation of the murine Pten tumor suppressor gene. *Genesis*. 2002;32(2):148–149.